Geometric considerations of the evolution of magnetic flux ropes

D. B. Berdichevsky,[1,2] R. P. Lepping,[2] and C. J. Farrugia[3]
[1]*L-3 Communications EER Systems, Inc., Largo, Maryland 20774*
[2]*NASA/Goddard Space Flight Center, Greenbelt, Maryland 20771*
[3]*Space Science Center, University of New Hampshire, Durham, New Hampshire 03824*
(Received 6 April 2002; revised manuscript received 2 December 2002; published 19 March 2003)

We use flux conservation and magnetohydrodynamics (MHD) theory to discuss essential differences in the nature of the evolution of two analytical solutions describing magnetic flux tubes evolving in time. The first of these maintains the elongation of the tube, while the second maintains a constant angular extension with respect to a possible pointlike source. In the first case, free expansion of the plasma (density N) occurs only in a direction perpendicular to the flux-tube x axis. In the second case, isotropic evolution is considered. In both cases it is assumed that at initial time t_0 the flux-tube **B** field is the force-free magnetostatic Lundquist solution, which energetically corresponds to the most stable state for any flux-tube structure. We show that for each case conservation of magnetic flux is enough to establish the scaling with time of the **B** field. While both expansions may correspond to the evolution of observed flux tubes in the heliosphere, the isotropic expansion appears to capture consistently essential features associated with the actual observations of expanding coronal mass ejections within 30 solar radii. For isotropic expansion of the plasma the force-free nature of the **B** field is preserved for all time. As an example the MHD solutions are applied to an interplanetary magnetic cloud observed with the spacecraft Wind, which passed Earth's vicinity on June 2, 1998.

DOI: 10.1103/PhysRevE.67.036405 PACS number(s): 95.30.Qd, 52.30.Cv, 96.50.Bh

I. INTRODUCTION

In the vicinity of Earth, the relatively frequent occurrences of convected solar wind regions with low proton β in good causal connection with solar coronal mass ejections (CMEs) with durations from many hours to a few days earlier at the Sun (see, e.g., Refs. [1], [2]) has been well documented. (In plasma physics β is the ratio of the plasma kinetic to magnetic-field energy densities.) A major effort has been devoted to the study of CME evolution through modeling and numerical solutions of the related magnetohydrodynamics (MHD) equations [3,4,5,6]. Frequently, these CME solar wind counterpart regions (ejecta) are amenable to identification as force-free flux tubes, [7] i.e., interplanetary magnetic clouds (IMC) [1,2]. (These flux tubes show increasing magnetic-field pitch angle as we probe plasma farther away from the axis of the tube. They are identified as flux ropes in heliospheric physics and we use this common terminology from here on.) These are transient, noncorotating, convected structures, moving as a whole away from the sun at a speed greater than 300 km s^{-1}, about 3 times the Alfvén speed V_A $(=B/\sqrt{N})$, while expanding at $\sim\frac{1}{2}\,V_A$ or less. The literature on the subject has been presented in its historical perspective and current understanding (see Refs. [8], [9] and references therein). Recently, some of the main characteristics of flux ropes have been recreated in the laboratory [10]. Some interplanetary flux ropes also appear to be related to the most extreme geomagnetic disturbances (see, e.g., ''bastille day'' Sun-Earth connection, Ref. [11]). Force-free magnetic-field structures have also been identified as stable magnetized plasma entities of astrophysical interest [12,13]. General conditions for their evolution have been analyzed [14]. In the case of an expanding flux rope, Suess [15] argued for buoyancy to explain the expansion process as the rope moves from a denser location near the Sun to the more tenuous regions of outer space. In this work, we consider the cases

$$\mathbf{V}(\mathbf{X},t)=(\rho/t)\mathbf{e}_\rho\,, \tag{1a}$$

$$\mathbf{V}(\mathbf{X},t)=(\rho/t)\mathbf{e}_\rho+(x/t)\mathbf{e}_x\,, \tag{1b}$$

i.e., the *free expansion* of an initially force-free, magnetostatic, Lundquist tube [16], where $\mathbf{V}(\mathbf{X},t)$ is the velocity of a specific element of plasma at location $\mathbf{X}$ $(=\rho\mathbf{e}_\rho+x\mathbf{e}_x)$ in the flux rope, $\mathbf{e}_x$ and $\mathbf{e}_\rho$ are the unit vector along and perpendicular to the observed flux-rope axis. Equations (1a) and (1b) are special cases of two-dimensional evolution conditions and t is the current time, equal to the addition of an arbitrary initial time t_0 plus the elapsed time interval $\Delta\tau$, i.e., $t=t_0+\Delta\tau$. These *free expansion Ansätze* appear common to ejecta observed in the interplanetary medium, as suggested by the solar wind velocity measured at different plasma locations inside the ejecta region, and their relationship to the time of lift-off at the Sun [17]. Equation (1a) and more general velocity laws with only a radial component have been discussed in several articles [18,19], and an example consistent with Eq. (1a) is given of the rope's magnetic-field evolution in the range ~0.3–5.0 AU (see, e.g., Refs. [20], [21]). Figure (1a) presents a sketch of this evolution with time t. In contradistinction with Eq. (1a) Kumar and Rust [9] discuss the role of an expansion in radius and elongation of a complex curvilinear flux rope. In our analysis this corresponds to Eq. (1b). Equation (1b) adds stretching along the axis to the radial expansion of Eq. (1a). Evolution of a flux-rope characterized by Eq. (1b) is consistent with the example in plate I by Hundhausen [22] and in most LASCO/SOHO coronograph image observations of limb CMEs [23]. It is likely that

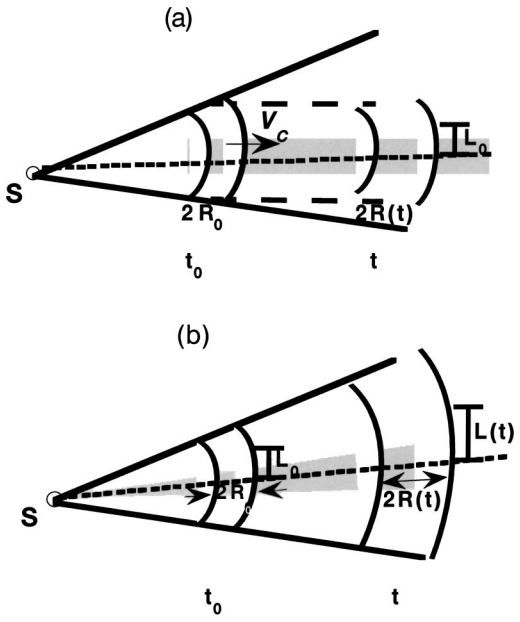

FIG. 1. View from the side of a flux rope at times t_0 and t, assumed to have emanated from source S (e.g., the sun) at time $t=0$. Shaded area indicates regions assumed to have negligible curvature. The arrow in the top panel indicates the direction of the convection velocity $\mathbf{V}_C$ of the tube. (a) A sketch, in arbitrary units, of the instantaneous shapes of a flux rope at times t_0 and t for evolution $R(t)$ only, Eq. (1), no expansion in elongation $[L(t)=L_0]$. (b) Same as (a) but for a flux rope that expands, i.e., evolves in time changing both in radius $R(t)$ and elongation $L(t)$ spanning a constant angle θ.

this isotropic expansion law is consistent in many cases with the expansion of magnetic clouds, at further distances from the Sun [23–25].

Magnetic flux conservation arguments are presented in Sec. II, a full MHD analysis is discussed in Sec. III, an example of one point observation and analysis of a flux rope in an interplanetary magnetic cloud time interval is presented in Sec. IV, and conclusions are drawn in Sec. V.

II. CONSIDERATIONS ON MAGNETIC FLUX CONSERVATION

In the following discussion, we will neglect the curvature of the magnetic flux rope, as is indicated in the sketches presented in Fig. 1. (Here, we limit ourselves to make local predictions. Note that in the large scale, curvature is assumed to be present.) Under this simplifying assumption the rope is a right cylinder of circular cross section with radius $R(t_0)$ at time t_0. We next assume that at time t_0, we have a minimum energy force-free flux-rope structure [12,18], hence, $\mathbf{J}=\alpha\mathbf{B}$, where $\mathbf{B}$ is the magnetic field, $\mathbf{J}$ is the $\mathbf{B}$-field aligned current, and α is a proportionality function of time. The corresponding expression of the $\mathbf{B}$ field for the cylindrical shape is

$$\mathbf{B}=B_0[Hg(t_0)J_1(\alpha(t_0)\rho)\mathbf{e}_\phi+f(t_0)J_0(\alpha(t_0)\rho)\mathbf{e}_x], \quad (2)$$

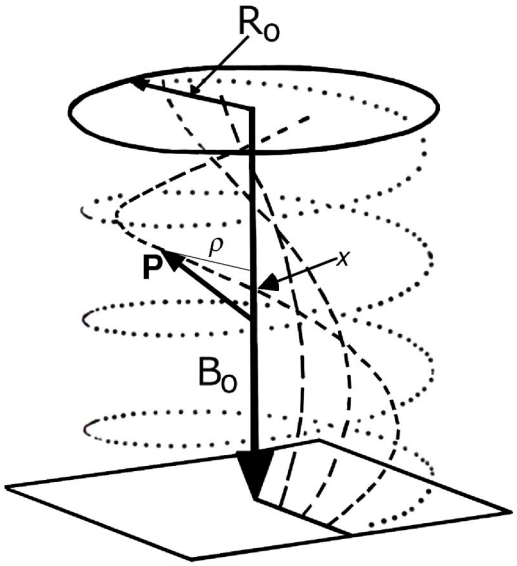

FIG. 2. Cylindrical representation, at time t_0, of an ideal force-free magnetic flux rope in terms of a nested set of magnetic-field lines (dashed and dotted) of various pitches growing more severely inclined as they depart from the rope's axis. B_0 is the magnetic-field strength on the axis, and R_0 is the radius of the rope. $\mathbf{X}$ is the displacement vector from the origin (on the axis) to the *plasma point P* in terms of the coordinates (ρ,x), where x is parallel to the axis and ρ is the radial coordinate. The solid oval at the top represents the cross section of the outer boundary of the rope.

with time evolution functions $f(t)$ and $g(t)$ equal to one at t_0. *Thus*, we have components $B_\phi(t_0)$ $[=HB_0J_1(\alpha(t_0)\rho)]$ and $B_x(t_0)$ $[=B_0J_0(\alpha(t_0)\rho)]$, where $H=\pm1$ is the rope's handedness, B_0 constant, and J_i are the $i=0,1$ order Bessel functions of the first kind [16]. We use a coordinate system with ρ and x directed, respectively, perpendicular and along its main axis and its origin rigidly attached to the center of the tube (see Fig. 2).

A flux rope of radial extension $R(t)$, to the point where the axial magnetic field is zero implies that $\alpha=2.4048/R$ (Table 9.5 in p. 409 in Ref. [26]). The quantity α which is inverse to $R(t)$, is in this way explicitly dependent on time t. Use of the conservation of magnetic flux suffices to obtain, from Eq. (2), the evolution of the flux rope magnetic field with time. Integrating the flux components between 0 and R, and $-L/2$ and $L/2$ gives

$$\Phi_\phi=HB_0g(t)\int_0^R\int_{-L/2}^{L/2}J_1(\alpha\rho)d\rho\,dx$$

$$=[HB_0g(t)/\alpha]L[1-J_0(\alpha R)], \quad (3a)$$

and

$$\Phi_x=B_0f(t)\int_0^R\int_0^{2\pi}J_0(\alpha\rho)\rho\,d\rho\,d\phi$$

$$=[B_0f(t)/\alpha^2](2\pi)/[\alpha RJ_1(\alpha R)]. \quad (3b)$$

Hence, Eqs. (3) give $\Phi_\phi=H0.4158B_0g(t)RL$ and $\Phi_x=1.3564B_0f(t)R^2$.

When only free radial expansion occurs, Eq. (1a), the radius of the flux rope grows at time t to be $R(t)=R(t_0)t/t_0$ $[R(t_0)\equiv R_0]$. The flux-rope elongation does not grow, i.e., $L(t)=L(t_0)$ $(\equiv L_0)$, hence, we find $g(t)=t_0/t$, and $f(t)=t_0^2/t^2$, and we obtain

$$\mathbf{B}=HB_0(t_0/t)J_1(\alpha(t)\rho)\mathbf{e}_\phi+B_0(t_0/t)^2J_0(\alpha(t)\rho)\mathbf{e}_x. \tag{4}$$

Then it is easy to check that Maxwell equation $\mathbf{J}=\boldsymbol{\nabla}\times\mathbf{B}$ gives $\mathbf{J}\|\mathbf{B}$ (force-free condition) only at time $t=t_0$ [19]. Hence, the geometry of the expansion imposes a solution that starts force-free but evolves away from it with time $t>t_0$. As shown in Sec. III, this implied solution to the **B** field is an approximate solution to the ideal MHD equations.

In the case of the expansion in radius and elongation of Eq. (1b), $L(t)=L_0\ t/t_0$ [similar to $R(t)=R(t_0)t/t_0$] with the result that [11] $g(t)=f(t)=t_0^2/t^2$, therefore, in this case,

$$\mathbf{B}=B_0(t_0/t)^2[HJ_1(\alpha(t)\rho)\mathbf{e}_\phi+J_0(\alpha(t)\rho)\mathbf{e}_x], \tag{5}$$

at $t\geqslant t_0$. This is the necessary time evolution for the poloidal and axial fields for force-free evolution of the **B** field to be possible.

Of equal interest are the density and pressure scaling with time. In the case of the density, we may assume mass conservation and plasma uniformly distributed over the whole volume of the flux rope. Thus, the scaling of density with time, i.e., particle number per volume (N), is proportional to the inverse of the volume (v) of the magnetic flux rope, and the following proportionality in time holds, $N(t)v(t)=N(t_0)v(t_0)$, i.e.,

$$N(t)=N(t_0)R_0^2L_0/R^2L=N(t_0)[t_0/t]^n, \tag{6}$$

with $n=2$ for radial expansion only, Eq. (1a), and $n=3$ in case of expansion on radius and elongation, Eq. (1b). Pressure scaling for an isothermal expansion of this dilute gas is then $P(t)=P_0[t_0/t]^n$, where, in general, for a gas with polytropic index γ

$$P(t)=P(t_0)[t_0/t]^{n\gamma}. \tag{7}$$

[We should mention here that other density (N) distributions can be successfully employed.] The evolutions of the magnetic flux-rope parameters with time are synthesized in Fig. 3.

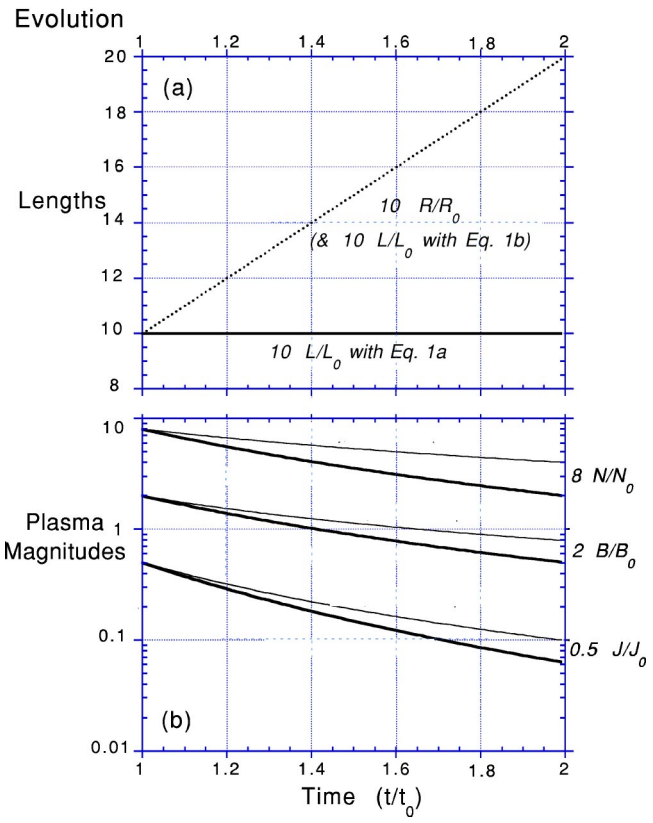

FIG. 3. (a) Time evolution between t_0 and $2t_0$ of the magnetic flux rope's dimensionless length ratios R/R_0 and L/L_0, scaled with a factor 10. (b) Time evolutions, relative to their t_0 values at *any* plasma location in the flux rope, of the plasma density N and the magnitudes of the magnetic (**B**) and current (**J**) fields. Thin, thick solid lines correspond to the expansion of Eqs. 1(a) and 1(b), respectively.

III. SELF-CONSISTENT MHD SOLUTIONS

Next we apply the MHD equations to the vector fields **V**, **B**, **J**, and scalar fields N, P. In case of radial expansion only, after entering **V**, **B**, N, P [Eqs. (1a) and (4), and case $n=2$ in Eqs. (6) and (7)] in the momentum equation,

$$N\partial_t\mathbf{V}+\mathbf{N}(\mathbf{V}\cdot\boldsymbol{\nabla})\mathbf{V}=+(\mathbf{J}\times\mathbf{B})-\boldsymbol{\nabla}P, \tag{8}$$

we find that the left hand side is identically zero, while the right hand side in Eq. (8) is given by $\mathbf{J}\times\mathbf{B}=[(\boldsymbol{\nabla}\times\mathbf{B})\times\mathbf{B}]=-B_0^2/R_0J_1(\alpha(t)\rho)J_0(\alpha(t)\rho)[(t_0/t)^3-(t_0/t)^5]\mathbf{e}_\rho$ and $-\boldsymbol{\nabla}P$. Hence, $-\boldsymbol{\nabla}P$ has to be equal to $\mathbf{J}\times\mathbf{B}$. In the asymptotic limit for times $t\gg t_0$, when $\mathbf{J}\times\mathbf{B}\approx 0$, the cold plasma condition can be used. For this asymptotic limit Eqs. (1a), (4), (6), and (7) are solution of the momentum equation. (Under more general considerations, in Ref. [27], the exact time evolution has been shown numerically, with the result that expansion occurs for $\gamma<1$, and that in its asymptotic limit the free expansion corresponds to the case when the value of γ is $\frac{1}{2}$ for $t\gg t_0$.)

$$\boldsymbol{\nabla}\cdot\mathbf{B}=0 \tag{9}$$

is satisfied because **B**, Eq. (4), is only dependent on t and ρ, and has component zero along $\mathbf{e}_\rho$. The free expansion with **V**, and $N(t)$, case $n=2$, in Eqs. (1a) and (6), satisfy identically the mass conservation condition

$$\partial_t N+\boldsymbol{\nabla}\cdot(N\mathbf{V})=0. \tag{10}$$

The Faraday equation $\partial_t\mathbf{B}=\boldsymbol{\nabla}\times\mathbf{E}$ in the ideal MHD limit $(\mathbf{E}=\mathbf{V}\times\mathbf{B})$ is equivalent to the flux conservation condition of Eq. (3). This allows solving in straightforward manner for the magnetic vector potential **A**, i.e.,

$$\partial_t\mathbf{A}=\mathbf{V}\times\mathbf{B}+\boldsymbol{\nabla}\Phi. \tag{11}$$

Because there are no free charges, $\nabla \cdot \mathbf{A}=0$ is required [28]. In the case of expansion only perpendicular to the x axis of the rope, the component $(\mathbf{V}\times\mathbf{B})_\rho$ is zero, and a consistent choice is $\Phi=0$. Direct integration at fixed $\mathbf{X}$ of Eq. (11) gives

$$\mathbf{A}(\rho,t)=B_0R_0[t_0/tJ_1(\alpha(t)\rho)\mathbf{e}_\phi+HJ_0(\alpha(t)\rho)\mathbf{e}_x], \tag{12}$$

and applying $\mathbf{B}=\nabla\times\mathbf{A}$, we recover the *non-force-free* magnetic field of Eq. (4). Finally the energy equation of the magnetized gas can be written as

$$N\,\partial_t\varepsilon+P\nabla\cdot\mathbf{V}+N\mathbf{V}\cdot\nabla\varepsilon=\mathbf{J}\cdot\mathbf{E}, \tag{13}$$

where ε is the gas thermal energy. In the non-force-free case, Eq. (1a), Joule heating $(\int_{V(R)}\mathbf{J}\cdot\mathbf{E}dV)$ is present, and its value scales with $(1/t)[1-(t_0^2/t^2)]/[(t_0^2/t^2)+0.12]$. Often, in spacephysics and astrophysics $t_0\geqslant 32$ h can be used and for this value of t_0 the Joule heating will be at any time less than 0.0013% of the magnetic-field energy. For $t\gg t_0$ it is possible to use the assumption $\nabla P=0$, which gives the temporal dependence on P of Eq. (7), for $n=2$, as our asymptotic solution to Eq. (13), while a more general solution can be found [27].

In the case of *isotropic* expansion of the plasma we prove the MHD Eqs. (8)–(11), and (13) with $\mathbf{V}$, and $\mathbf{B}$ in Eqs. (1b) and (5), and N and P, for $n=3$, in Eqs. (6) and (7). It is straightforward to show that they are exact solution of the MHD equations. Here, we focus on the condition on the magnetic-field vector potential, $\nabla\cdot\mathbf{A}=0$. It imposes the solution $\Phi=-HB_0(t_0/t)^2/(\alpha_0 t_0)\ xJ_0(\alpha(t)\rho)$ in Eq. (11), and through direct integration of Eq. (11) at fixed $\mathbf{X}$ gives

$$\mathbf{A}(\rho,t)=B_0(R_0t_0/t)[J_1(\alpha(t)\rho)\mathbf{e}_\phi+HJ_0(\alpha(t)\rho)\mathbf{e}_x]. \tag{14}$$

IV. APPLICATION TO THE JUNE 2, 1998 MAGNETIC CLOUD

We now apply the above ideas to a flux rope observed on June 2, 1998 from 180 Earth radii upstream of the Earth. The data used where 1 min magnetic field averages for the MFI instrument in the spacecraft Wind, and 15 s proton moment distribution values evaluated every 92 s. Absolute magnetic-field uncertainty is a fraction of nanotesla (nT). The relative uncertainty of the used magnetic-field vector is well within the thickness of the line of the plots used for their presentation. Absolute error in the plasma quantities are 1% for the solar wind velocity, and 5% and 15%, respectively, for N and the temperature T. Relative errors in $\mathbf{V}$, N, and T, under the solar wind conditions studied are estimated to be less than 0.1%, 0.2%, and 0.3%, respectively. (In the case of N, we checked that the proton profile particle numbers per cm^3 presented here coincide with the same Wind SWE evaluated plasma number measured with the electron detector, and a method based on the thermal electron oscillation mode, called plasma line, and measured with the Wind WAVES instrument.) Vector quantities are given in geocentric solar ecliptic (GSE) coordinate system [29]. An electron temperature estimate is obtained from Wind SWE high-resolution electron data (3 s averages every 12 s), used for the calculation of the mean plasma β.

Field and plasma data are shown in Fig. 4. From top to bottom the panels show (a) magnitude of the magnetic field, (b) its orientation with respect to the plane of the ecliptic (latitude), and (c) in the ecliptic plane (longitude), (d)–(f) magnitude of the velocity of the solar wind and its orientation in latitude and longitude, (g) mass number (protons), and (h) electron and proton temperature. In the interval 9:30–15:54 UT, panel (a) shows that the magnetic field is stronger than normal, it executes a large rotation [panel (b)] and the proton temperature T_p is low (bottom panel). These characteristics indicate a magnetic cloud [8]. In addition, the bottom panel in Fig. 4 shows that the flux rope is immersed in a heat bath provided by the electron gas. See the overall smooth profile of the electron temperature ($T_e\sim 10^5$ K) slowly decreasing in time and its ratio to the proton temperature ($T_e/T_p\sim 3$). Therefore, it suggests that in this case $\nabla P\approx 0$. Is this consistent with any of the geometric considerations in Eq. (1), and Sec. II? We investigate it through the analysis of this example. (This T_e/T_p ratio, and the mean plasma $\beta\leqslant 1/4$ are consistent with observations in other interplanetary magnetic clouds at 1 AU.)

The (static) Lundquist model fit [16] is shown by the solid lines in panels (a)–(c). It can be seen that this generally fits the magnetic data well, particularly near the center interval. The results of the fitting routine in the orientation of the flux tube and its closest approach are: $\phi_A=55°$ with respect to the Sun-Earth direction (longitude), $\theta_A=25°$ in its inclination with respect to the ecliptic (latitude), and a closest approach $d/R_s=0.3$. This Lundquist's fit has a small asymmetry factor of 3.8%, and a quality better than usual. Clearly, for a static solution constant plasma parameters are required and these are shown with solid lines in panels (d)–(g). Toward the time boundaries, that correspond to the leading edge and the trailing end of the flux-rope passage, the observational field and plasma parameters show larger deviations from the static model than the middle region. For this flux rope, moving with a mean speed of 405 $\mathrm{km\,s^{-1}}$, a static radius of $R_s=4.6\times 10^6$ km is obtained. Notice that this case belongs to a group of magnetic clouds showing a rather gentle interaction with its surroundings making it a good example for comparison with the models discussed in the previous sections. Nevertheless, there are some signatures of interaction with the ambient medium. In this regard, we mention the upstream pressure pulse (PP) passage between 8:20 and 8:22 UT on June 2, 1998 characterized by enhancement in the interplanetary magnetic field (IMF), plasma density number N, and proton temperature T_p lasting until the encounter at 9:30 UT of the leading edge of the IMC (flux rope). At passage time, the PP is a perturbation propagating locally at a speed less than the magnetosonic speed and likely driven by the flux rope as a result of its interaction with a slightly slower solar wind stream ahead.

We next model the expansion of the magnetic cloud assuming that it originates at the Sun. We divide the distance 1 AU (from the Sun) with the local mean velocity of the cloud ($\approx$405 $\mathrm{km\,s^{-1}}$) to find the time t_0 ($\approx$100 h), after subtraction

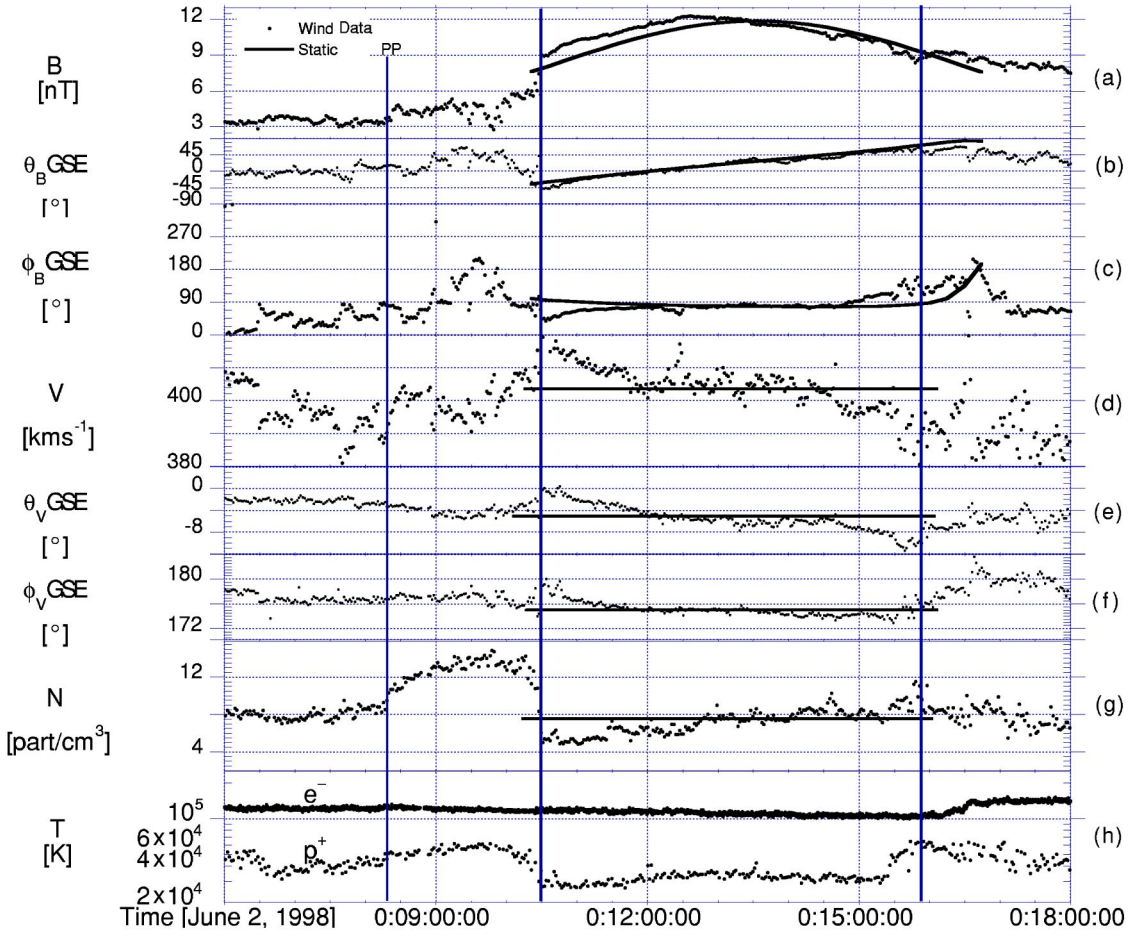

FIG. 4. The time profiles of the IMF and SW plasma parameters at Wind (~1 min averages) from 6 to 18 UT on June 2, 1998. The panels from top to bottom represent: (a) the magnitude of the IMF, B; (b) the latitude angle θ_B of the IMF; (c) the azimuth angle ϕ_B of the IMF; (d) the SW speed V (protons); (e) the latitude angle θ_V of the SW velocity; (f) the azimuth angle ϕ_V of the SW velocity; (g) the SW proton number per cm N_p; and (h) electrons (e^-) and protons (p^+) temperature. The static flux-rope solution [1] is given by the solid line in panels (a)–(c). Plasma conditions, consistent with a MHD structure constant in time, are indicated by the horizontal solid lines of panels (d)–(g). During the interval of observations $\mathbf{X}_{\rm GSE}$, $\mathbf{Y}_{\rm GSE}$, $\mathbf{Z}_{\rm GSE}=180$, 45, 21 Earth radii, respectively, give the spacecraft location (Wind). PP indicates a pressure pulse. Other solid vertical lines indicate the start and end of the flux-rope time interval, see discussion.

of half its time passage $\Delta\tau$ (=5.4 h). (t_0 is the time from launch to the local observation of the passage of the leading edge of the IMC.) At the trailing end of the magnetic cloud the time ($t=t_0+\Delta\tau$) is ≈105.4 h. To estimate ΔV and R_0, we use

$$\Delta\mathbf{V}=\mathbf{V}(t_0)-\mathbf{V}(t_0+\Delta t)$$
$$=-(R_0/t_0)\mathbf{e}_{\rm in}+(R_0/t_0)\mathbf{e}_{\rm out}+2(X_0/t_0)\mathbf{e}_x,$$

i.e.,

$$\Delta V=2R/t_0 \quad \text{with} \quad R=\sqrt{R_0^2(1-\mathbf{e}_{\rm in}\cdot\mathbf{e}_{\rm out})/2+X_0^2}, \quad (15)$$

where X_0 [$=R_0/\tan(\alpha)$] is the corresponding distance along the axis of the flux rope ($\mathbf{e}_x$), where α [$=\arccos(\cos\phi_A\cos\theta_A)$] is the angle between the trajectory vector ($\approx -X_{\rm GSE}$) and the flux rope's axis. The directional vectors $\mathbf{e}_{\rm in}$ and $\mathbf{e}_{\rm out}$ are perpendicular to the cloud axis and point to the leading and rear boundaries of the flux rope. The angle between $\mathbf{e}_{\rm in}$ and $\mathbf{e}_{\rm out}$ is defined by the spacecraft trajectory at a constant distance $Y_0=-0.3R_0$ from the cloud axis (x in cloud coordinates). $\Delta\tau$ is given by the relationship

$$\Delta\tau=t_0R_0/(t_0V_{\rm CA})[2+3R_0/(t_0V_{\rm CA})+2R_0/(t_0V_{\rm CA})^2]$$
$$+O(t_0^{-3}). \quad (16)$$

Equations (15) and (16) give our estimated values $R_0=3.6\times10^6$ km, and $V_{\rm CA}=\Delta V=21\ {\rm km\,s^{-1}}$. These values compare well with the static R_s and reproduce the observed gradient in the solar wind speed. For the computation of the variable t, argument in the flux-rope model quantities $\mathbf{V}_{\rm MC}$, $\mathbf{B}_{\rm MC}$ and scalar $N_{\rm MC}$, we use

$$\Delta\tau_{\rm CAin}\approx R_0/V_{\rm CAin}\left[1+\frac{1}{t_0}\frac{R_0}{V_{\rm CAin}}+\left(\frac{1}{t_0}\frac{R_0}{V_{\rm CAin}}\right)^2+O(t_0^{-3})\right]$$

and

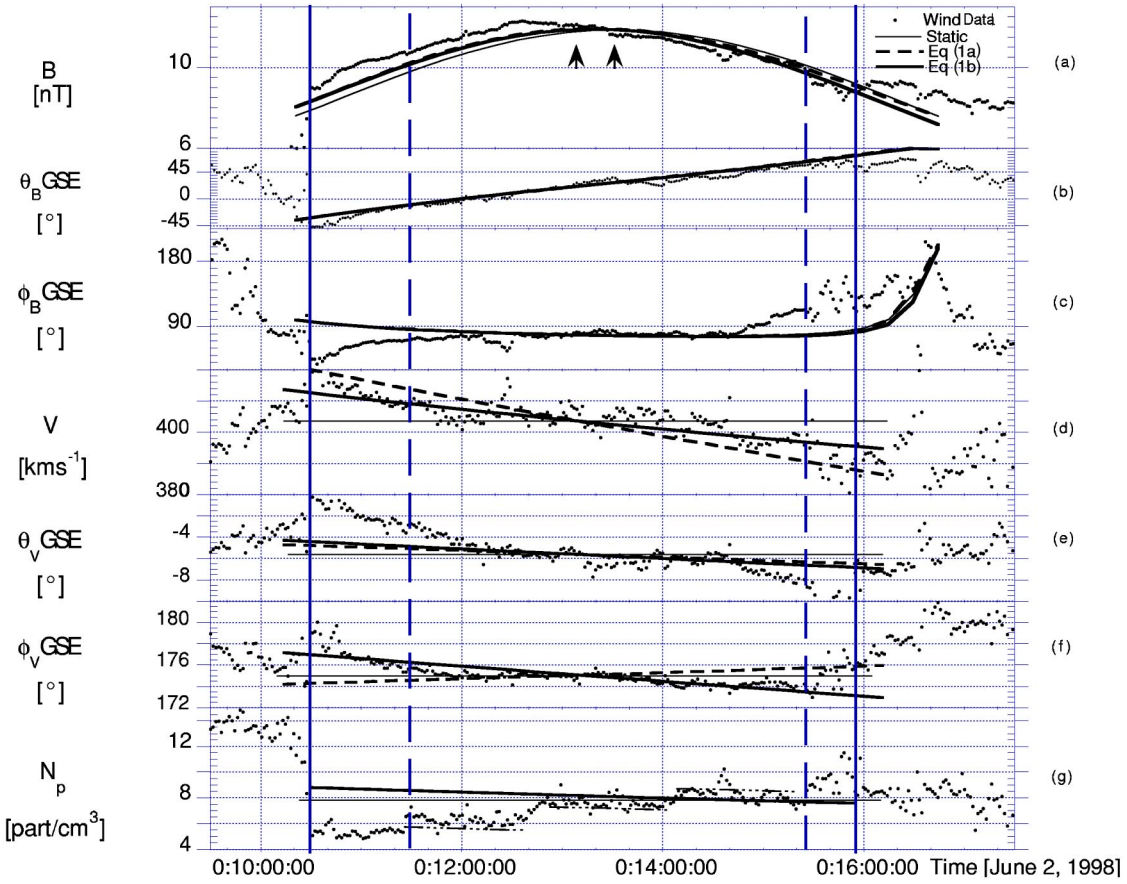

FIG. 5. Presented is a more detailed view, for a shorter time interval, of the time profiles of plasma parameters displaying the flux-rope observations of Fig. 4 (no $T_{p,e}$). It shows dynamic changes against observation (dots) and the static fit (thin solid lines). Arrows in the top panel mark the shift in the maximum value of B from ~1332 UT for the static [1] to an earlier time (~1307 UT) for the MHD solutions. Each panel displays the time profiles for the MHD solutions corresponding to the plasma expansion laws: (1) of Eq. (1a) dashed lines; and (2) of Eq. (1b), solid lines. From left to right, the solid to dashed, dashed to dashed, and dashed to solid vertical lines delimit, respectively, the front, middle, and rear time intervals discussed in the text. Long dash-three dots segments in the middle time interval of the bottom panel give the MHD time profile for the evolution of a *simple* axial symmetric N.

$$\Delta\tau_{\mathrm{CAout}} \approx R_0/V_{\mathrm{CAin}}\left[1+2\frac{1}{t_0}\frac{R_0}{V_{\mathrm{CAin}}}+\left(\frac{1}{t_0}\frac{R_0}{V_{\mathrm{CAin}}}\right)^2+O(t_0^{-3})\right].$$

The quantities $\Delta\tau_{\mathrm{CAin}}$ and $\Delta\tau_{\mathrm{CAout}}$ are defined to be the time interval from entry to closest approach (CA) and CA to exit of the flux rope, respectively. Hence $\Delta\tau_{\mathrm{CAin}}$ and $\Delta\tau_{\mathrm{CAout}}$ are scaled to the start and end times of the observed time passage of the cloud. Then by iterating the partition of $\Delta\tau_{\mathrm{CAin}}$ and $\Delta\tau_{\mathrm{CAout}}$, we obtain the time evolution of the expanding flux rope. Now for a comparison with observation we rotate $\mathbf{V}_{\mathrm{MC}}$ and $\mathbf{B}_{\mathrm{MC}}$ from cloud (cl) to GSE coordinate.

Figure 5 shows detailed displays of the expanding MHD solution, corresponding to the velocity expansion fields of Eqs. (1a) and (1b), both in comparison to the field and plasma observations. The changes with respect to the static solution of the flux rope [16] are also presented. The analytical MHD evolution models show marked improvement: (1) The location of the maximum in the magnitude of the magnetic field; it shifts from 13:32 to 13:07 UT (see arrows in top panel); (2) Gradient in $\mathbf{V}$ and its angular components are partly reproduced [panels (d)–(f)]. (Overall the velocity appears to be better represented by the force-free evolution of Eq. (1b), whereas some subintervals appear to be well represented by the non-force-free MHD evolution of Eq. (1a) or the static solution. There is little effect on the magnetic-field angles [panels (b) and (c)], despite a 1.6% asymmetry respect to the axis between entry and exit points.) The observed density appears to be structured instead of isotropic as assumed in the model derivations. For this density profile, we can assume a cylindrically symmetric shape making it fit in the set of functions consistent with the $\mathbf{B}_{\mathrm{MC}}$, and $\mathbf{V}_{\mathrm{MC}}$ MHD evolutions derived in Sec. III. Here, we focus on the structures of N_{MC} observed between vertical dashed lines in Fig. 5, bottom panel, where for each of the N_{MC} structures dot-dashed segments highlight an evolution consistent with the rate of expansion of the velocity $\mathbf{V}_{\mathrm{MC}}$ derived above.

As we show next using momentum [Eq. (8)], a better representation of observations with the force-free solution is expected. Equations (1a) and (1b) make the left side of Eq. (8) zero. $\nabla P=0$, in the right side of Eq. (8), is very well supported with the observation of an overall, slightly, steady decrease of T_e with time, and the ratio $T_e/T_p \approx 3$ (Fig. 4).

Therefore, $\mathbf{J}\times\mathbf{B}=0$, gives the right solution. The deviations near the flux-rope boundaries between models and observational parameters remain. This effect is particularly noticeable in B, ϕ_B, θ_V, and N in the front side region, and in ϕ_B, V, θ_V, and N in the rear side region. These are due, in our view, to interaction with the ambient medium, not modeled here (e.g., the front side distortions on the left, between solid and dash line, related to the PP ahead of the IMC, shown in Fig. 4). The IMC rear distortions on the right side, between dash and solid lines, appear to have a shorter duration consistent with an apparently gentler interaction with the ambient solar wind than in the flux rope's front side.

V. SUMMARY AND CONCLUSIONS

In Sec. II, we presented the time evolution of a circular, straight-cylindrical flux rope containing plasma which obeys the MHD equations for two different free-expansion *Ansätze* [Eqs. (1a) and (1b)]. The conservation of magnetic flux alone suffices to show that intrinsically different evolutions result for these cases, which are intimately related to the geometry of the chosen expansion law. It is straightforward to check using Eqs. (4) and (12), and (5) and (14) that magnetic helicity, given by $\int \mathbf{A}\cdot\mathbf{B}\, dV$, is also conserved. This is not the case for the magnetic energy ($\propto\int \mathbf{B}\cdot\mathbf{B}\, dV$), and here we conjecture that the freed magnetic-field energy—in the bulk of the tube—will be transferred to the plasma and eventually manifest itself in the form of heating and electromagnetic radiation. Heating effects on the plasma polytropic index would make it deviate from the ratio of the gas specific heats at constant volume and pressure (see, e.g., Ref. [30]). The analysis of the evolution of the thermodynamics of the plasma with time is beyond the scope of the paper and will be treated elsewhere. No conditions were imposed concerning plasma β, except for the requirement that $\nabla P\approx 0$ in the whole volume of the rope. This apparently restrictive condition is easier to satisfy in low β plasmas, at least approximately, when the plasma kinetic energy is much smaller than magnetic-field energy (i.e., cold plasma approximation, for $\beta\ll 1$).

Case studies support the MHD evolution of a flux rope maintaining its length [Eq. (1a)] over large distances [20,21]. Section IV shows observations at one location of a flux-rope passage with **B**, **V**, and N evolutions in time consistent with expansion at constant angle [Eq. (1b)] with respect to a launch at or near the Sun's surface, corresponding to sketch in the bottom part of Fig. 1. This is a case of finite β ($\leqslant 0.25$) and an overall featureless, slight, smooth decrease of the heat of the system with time, which is mostly contained in the electrons temperature. Although there are $\sim$2 min pressure fluctuations or pressure balance microstructures locally present, and it appears that heating is enabled (see, e.g., Sec. 6.7, in Ref. [8]). The study of this interesting thermodynamic medium is beyond the scope of the paper. Its understanding would require correlative analysis of high-resolution solar wind plasma parameters from multiple points of observation in space.

The here discussed force-free solution to evolution given by Eq. (1b), and other theoretical analyses appear consistent with the existence of more general force-free magnetic structures, e.g., magnetic tubes with nonzero curvature capable of growth in space as a function of time. (See, e.g., the study of magnetostatic force-free flux ropes with curvature, having a toroidal geometry [31].) Consequently we propose that some of the structures observed in (solar physics, space physics, and astro physics) physics could be close to the constant α force-free state. These results may also be of interest in astrophysics and controlled plasma fusion. Chandrasekhar and Woltjer [13] have emphasized stability of interstellar force-free magnetic structures with implications for the role of such structures, over extended time scales, in processes such as the scattering of cosmic rays. However, as it may be the case for a certain type of magnetostars, instabilities due to specific boundary conditions would strongly affect the life span of force free structures [32]. Instabilities in magnetically confined hot plasma, allowing for transients with the spatiotemporal evolution of force-free flux ropes, may represent a hurdle to be avoided in the search for *the* high temperature plasma conditions needed for the unhindered steady fusion process under human control.

Note added. After the writing of this paper it came to our attention that Shimazu and Vandas [33] also, with a different focus, present the force-free solution discussed in this work.

ACKNOWLEDGMENTS

We acknowledge partial support by NASA's LWS Grant No. NAG 5-10883 and by NSF Grant No. ATM-0208414.

[1] L. F. Burlaga, J. Geophys. Res. **93**, 4 (1988); **93**, 103 (1988).
[2] J. T. Gosling, edited by C. T. Russell, E. R. Priest, and L. C. Lee, Geophysical Monograph Vol. 58 (AGU, Washington, D.C., 1990), pp. 349–364.
[3] P. J. Cargill *et al.*, J. Geophys. Res. **101**, 4855 (1996).
[4] J. Chen, J. Geophys. Res. **101**, 27 (1996); **101**, 499 (1996); **101**, 519 (1996).
[5] S. T. Wu, W. P. Guo, and J. F. Wang, Sol. Phys. **157**, 325 (1995).
[6] S. T. Wu, M. D. Andrews, and S. P. Plunkett, Space Sci. Rev. **95**, 191 (2001).
[7] R. P. Lepping and D. B. Berdichevsky, in Recent Research Developments in Geophysical Research, Trivandrum-8, India, 2000, pp. 77–96 (unpublished).
[8] L. F. Burlaga, *Interplanetary Magnetohydrodynamics* (Oxford University Press, New York, 1995).
[9] A. Kumar and D. M. Rust, J. Geophys. Res. **101**, 15 (1996); **101**, 667 (1996); **101**, 684 (1996).
[10] P. M. Bellan and J. F. Hansen, Phys. Plasmas **5**, 1991 (1998).
[11] R. P. Lepping *et al.*, Sol. Phys. **204**, 287 (2001).
[12] L. Woltjer, Proc. Natl. Acad. Sci. U.S.A. **44**, 489 (1958).
[13] Chandrasekhar and Woltjer, Proc. Natl. Acad. Sci. U.S.A. **44**, 285 (1958).
[14] W.-H. Yang, Astrophys. J. **348**, L73 (1990).

[15] S. T. Suess, J. Geophys. Res. **93**, 5 (1988); **93**, 437 (1988).
[16] S. Lundquist, Ark. Fys. **2**, 61 (1950).
[17] D. B. Berdichevsky *et al.*, Ann. Geophys. **20**, 891 (2002).
[18] C. J. Farrugia *et al.*, J. Geophys. Res. **98**, 7621 (1993).
[19] V. A. Osherovich, C. J. Farrugia, and L. F. Burlaga, J. Geophys. Res. **98**, 13 (1993); **13**, 225 (1993); **13**, 231 (1993).
[20] V. A. Osherovich *et al.*, in Proceedings of the 31st ESLAB Symposium on Correlated Phenomena at the Sun, in Heliosphere and in Geospace, ESA-SP 415, 1997, pp. 171–175 (unpublished).
[21] C. J. Farrugia *et al.*, in *Solar Wind Seven*, edited by E. Marsch and R. Schwenn (Pergamon, New York, 1992), pp. 611–618.
[22] A. J. Hundhausen, in *Coronal Mass Ejections*, edited by N. Crooker, J.-A. Joselyn, and J. Feynman, Geophysical Monograph, Vol. 99 (AGU, Washington, DC, 1997), pp. 1–7.
[23] O. C. St. Cyr *et al.*, J. Geophys. Res. **105**, 18 (2000); **105**, 159 (2000); **105**, 185 (2000).
[24] L. F. Burlaga *et al.*, J. Geophys. Res. **86**, 6673 (1981).
[25] K. Marubashi, in *Coronal Mass Ejections*, edited by N. Crooker, J.-A. Joselyn, and J. Feynman, Geophysical Monograph, Vol. 99 (AGU, Washington, D.C., 1997).
[26] *Handbook of Mathematical Functions*, edited by M. Abramowitz and I. A. Stegun, 9th ed. (Dover, New York, 1972).
[27] V. A. Osherovich, C. J. Farrugia, and L. F. Burlaga, J. Geophys. Res. **100**, 12 (1995); **100**, 12 (1995); V. A. Osherovich and L. F. Burlaga, in *Coronal Mass Ejections* (Ref. [25]), pp. 157–168.
[28] J. D. Jackson, *Classical Electrodynamics* (Wiley, New York, 1962).
[29] W. H. Mish *et al.*, Space Sci. Rev. **71**, 815 (1995).
[30] G. Siscoe, in *Solar-Terrestrial Physics*, edited by R. L. Caravillano and J. M. Forbes (Reidel, Norwell, 1983), pp. 11–100; B. C. Low, J. Geophys. Res. **106**, 25 (2001); **106**, 141 (2001); **106**, 163 (2001).
[31] M. A. Hidalgo *et al.*, Sol. Phys. **194**, 165 (2000).
[32] D. A. Uzdensky, A. Königl, and C. Litwin, Astrophys. J. **565**, 1191 (2002).
[33] Hironori Shimazu and Marck Vandas, Earth Planet. Sci. J. **54**, 783 (2002).